Current Biology 17, 1817–1825, October 23, 2007 ©2007 Elsevier Ltd All rights reserved DOI 10.1016/j.cub.2007.09.032

Report

ESCRTs and Fab1 Regulate Distinct Steps of Autophagy

Tor Erik Rusten,[1,2] Thomas Vaccari,[3] Karine Lindmo,[1,2] Lina M.W. Rodahl,[1,2] Ioannis P. Nezis,[1,2] Catherine Sem-Jacobsen,[1,2] Franz Wendler,[4] Jean-Paul Vincent,[4] Andreas Brech,[1,2] David Bilder,[3] and Harald Stenmark[1,2,*]

[1]Centre for Cancer Biomedicine
University of Oslo
[2]Department of Biochemistry
The Norwegian Radium Hospital
Montebello
N-0310 Oslo
Norway
[3]Department of Molecular and Cell Biology
University of California, Berkeley
Berkeley, California 94720
[4]Medical Research Council National Institute for Medical Research
The Ridgeway
Mill Hill
London NW7 1AA
United Kingdom

Summary

Eukaryotes use autophagy to turn over organelles, protein aggregates, and cytoplasmic constituents. The impairment of autophagy causes developmental defects, starvation sensitivity, the accumulation of protein aggregates, neuronal degradation, and cell death [1, 2]. Double-membraned autophagosomes sequester cytoplasm and fuse with endosomes or lysosomes in higher eukaryotes [3], but the importance of the endocytic pathway for autophagy and associated disease is not known. Here, we show that regulators of endosomal biogenesis and functions play a critical role in autophagy in *Drosophila melanogaster*. Genetic and ultrastructural analysis showed that subunits of endosomal sorting complex required for transport (ESCRT)-I, -II and -III, as well as their regulatory ATPase Vps4 and the endosomal PtdIns(3)P 5-kinase Fab1, all are required for autophagy. Although the loss of ESCRT or Vps4 function caused the accumulation of autophagosomes, probably because of inhibited fusion with the endolysosomal system, Fab1 activity was necessary for the maturation of autolysosomes. Importantly, reduced ESCRT functions aggravated polyglutamine-induced neurotoxicity in a model for Huntington's disease. Thus, this study links ESCRT function with autophagy and aggregate-induced neurodegeneration, thereby providing a plausible explanation for the fact that ESCRT mutations are involved in inherited neurodegenerative disease in humans [4].

*Correspondence: stenmark@ulrik.uio.no

Results and Discussion

An increased understanding of the mechanisms that regulate macroautophagy (hereafter referred to as autophagy) is critical because the dysregulation of autophagy is seen in many human pathologies, including cancer and neurodegeneration [2, 5]. Insight into the molecular mechanisms of autophagy stems largely from genetic screens in yeast, which have identified two ubiquitin-like conjugation machineries necessary for autophagosome formation [1, 6, 7]. Although the requirement for these machineries has been conserved to higher eukaryotes, the molecular mechanisms of autophagic transport to the lysosomes in metazoans are less clear. In yeast, the autophagosome fuses directly with the vacuole (lysosome) in a step requiring the small GTPase, Ypt7/Rab7, the HOPS-C complex, and SNAREs [6, 8, 9]. In contrast, it is well established that fusion structures between autophagosomes and endosomal compartments, called amphisomes, are formed in higher eukaryotes [3, 10, 11]. This raises the question of whether autophagy in metazoans is controlled by components that regulate endosome biogenesis and sorting functions. Endosomal sorting complexes required for transport (ESCRTs) are interesting in this context because these complexes mediate multivesicular body (MVB) biogenesis and degradative protein sorting and because their dysfunction is associated with neurodegenerative disease in humans [4]. Another candidate regulator of autophagy is the PtdIns(3)P 5-kinase Fab1/PIKfyve, which controls late-endosomal membrane homeostasis, and whose inactivation is associated with an inherited form of fleck corneal dystrophy [12].

Autophagy in *Drosophila* is regulated by global nutritional and developmental cues such as amino acid availability and hormonal signaling [13, 14]. In order to overcome confounding effects from such systemic influences, we analyzed trafficking mutants in clones of cells by using surrounding wild-type cells as a control. Mutant clones were induced by FLP-FRT technology in animals expressing Gal4. The clones were recognized by the loss of a upstream activating sequence (UAS)-myristylated red fluorescent protein (mRFP) transgene present on the homologous chromosome. In order to follow autophagy, we used a transgene located on another chromosome that carries UAS-GFP-Atg8a (GFP: green fluorescent protein), which labels autophagosomes and autolysosomes (Figure 1A) [13, 15–17].

To address the role of the endosomal sorting machinery in autophagy, we selected flies containing null mutations in members of ESCRT-I (*vps28*), -II (*vps25*), and -III (*vps32*) obtained in a screen for tumor suppressors [18, 19] (T.V. and D.B., unpublished data). We first investigated clones of the ovarian follicular epithelium in stage 8 or 9 egg chambers, in which no autophagy is normally detectable. Interestingly, mutant follicular epithelial cells of *vps28*, *vps25*, and *vps32* all accumulated intracellular structures positive for GFP-Atg8a in a cell-autonomous

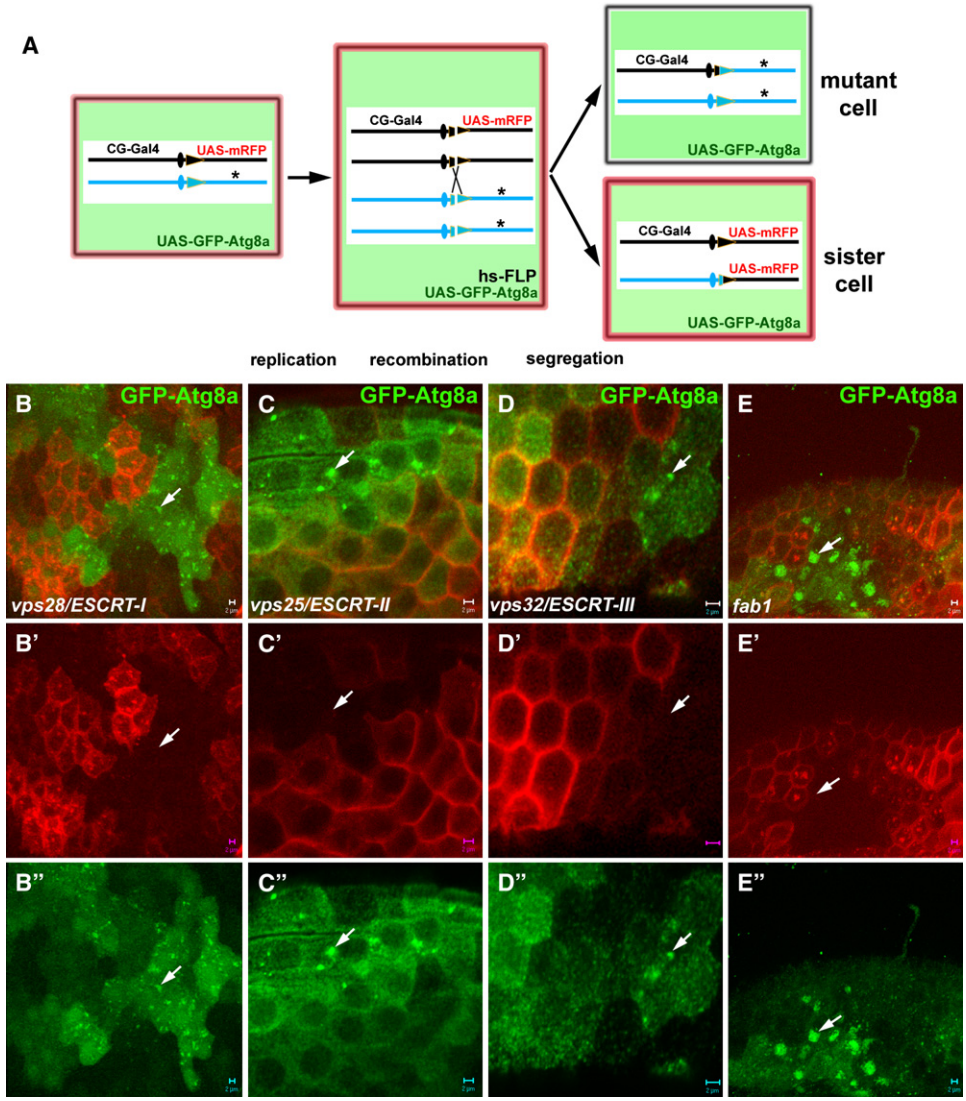

Figure 1. Accumulation of Autophagic Structures in *ESCRT* and *fab1* Mutant Follicle Cells

(A) Diagram showing cells from a heterozygous *Drosophila* for a given mutation (asterisk) expressing mRFP (red, plasma membrane) as a cell marker and GFP-Atg8a (green, cytoplasm) as a marker for autophagy under CG-Gal4 control. The transient expression of FLP recombinase (hs-flp) mediates the mitotic recombination of chromosome arms carrying FRT sites (triangles) situated close to the centromeres (ovals). Mutant cells are identified by the loss of mRFP. All cells still express GFP-Atg8a because it is carried on another chromosome (UAS-GFP-Atg8a).

(B–E) Distinct from control cells (red), follicle cells mutant for *vps28*, *vps25*, *vps32*, and *fab1* all show intracellular punctuate structures (arrows) labeled by GFP-Atg8 (B″, C″, D″, and E″), indicating the presence of autophagic membranes. Scale bars represent 2 μm. The genotypes are as follows: *y,w, hs-flp/+;FRT42D,vps28^{D2}/CG-Gal4, FRT42D, UAS-mRFP; UAS-GFP-Atg8a/+* (B), *y,w, hs-flp/+;FRT42D,vps25^{A3}/CG-Gal4, FRT42D, UAS-mRFP; UAS-GFP-Atg8a/+* (C), *y,w, hs-flp/+;FRT42D,vps32^{G5}/CG-Gal4, FRT42D, UAS-mRFP; UAS-GFP-Atg8a/+* (D), and *y,w, hs-flp/+; FRT42D,fab1^{21}/CG-Gal4, FRT42D, UAS-mRFP; UAS-GFP-Atg8a/+* (E).

manner (Figures 1B–1D). A similar appearance of GFP-Atg8a structures was observed when cells were made mutant for *fab1*, involved in late-endocytic trafficking and membrane homeostasis (Figure 1E) [20]. The accumulation of GFP-Atg8a in ESCRT and *fab1* mutant cells under nonstarved conditions suggested that autophagic structures accumulated as a result of steady-state, low-level autophagic sequestration coupled with incomplete digestion in these cells.

We next focused on ESCRT function in the fat body, the *Drosophila* counterpart of mammalian liver and adipose tissue, where the regulation of autophagy has been extensively studied. In well-fed stage L1, L2, and early L3 wild-type larvae, very little autophagy was observable in the fat body either by electron microscopy or with the GFP-Atg8a reporter. Nevertheless, as shown previously [13, 14], autophagy was rapidly induced in this tissue by amino acid starvation (data not shown). As in follicular epithelial cells, fat body cells lacking ESCRT components, but not their wild-type neighbors, accumulated GFP-Atg8a in subcellular structures even under nonstarved conditions (Figure 2A). The starvation of L2 larvae for 4 hr resulted in the appearance of autophagic structures in both the *vps25* mutant cells and surrounding control cells (Figures 2B and 2C). Together, these results confirm the data from the follicular epithelial clones

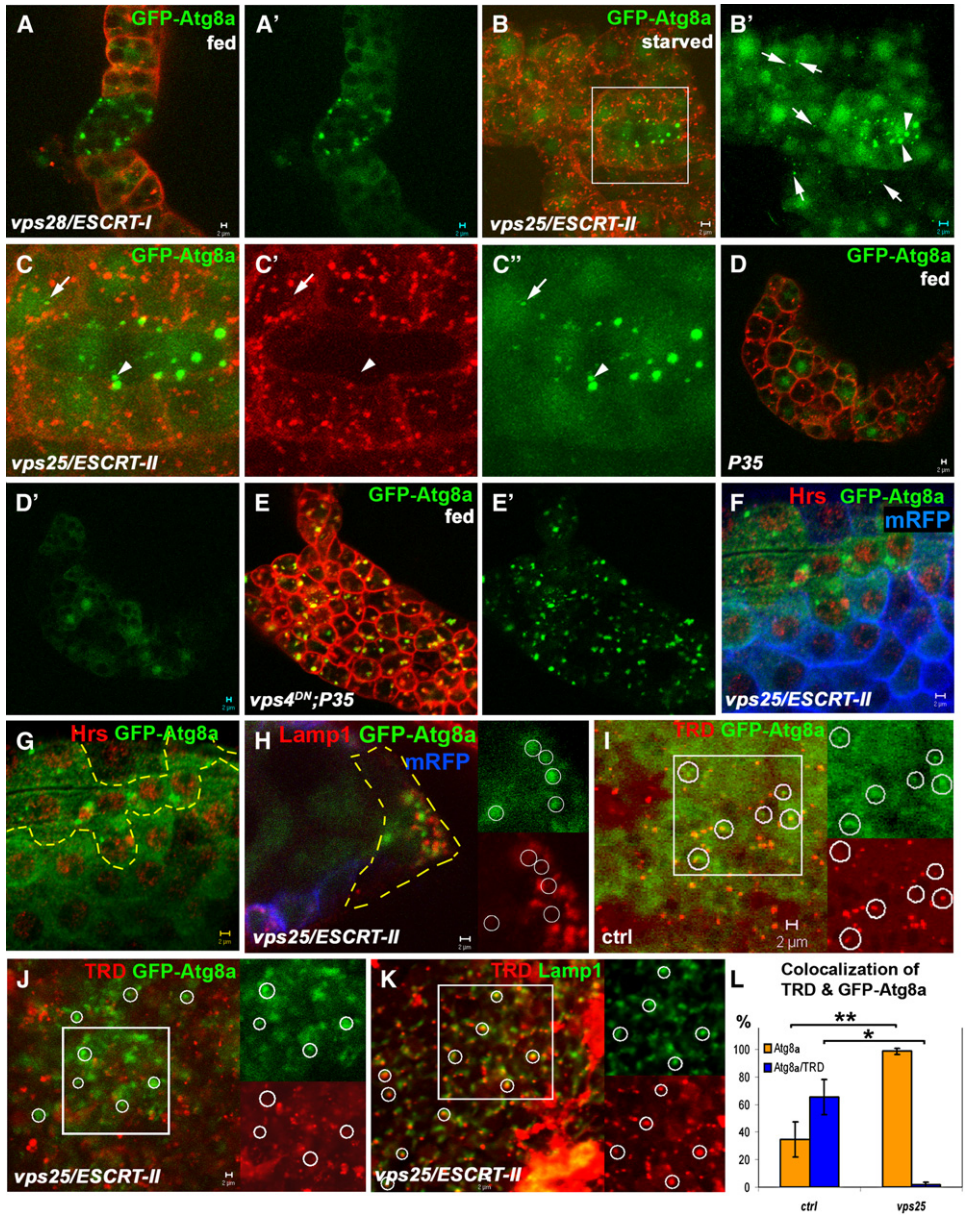

Figure 2. Autophagic Activity in Vps4^{DN}-Expressing and *ESCRT* Mutant Cells

(A) ESCRT mutant cells in the fat body of fed L1 larvae accumulate punctuate GFP-Atg8a structures, whereas neighboring control cells (red) do not.

(B and C) Unlike the situation in fed larvae, both ESCRT mutant (arrowhead) and surrounding control (red, arrow) cells show GFP-Atg8a accumulation in starved animals.

(D) No GFP-Atg8a accumulation is seen in fat body cells expressing the apoptosis inhibitor P35.

(E) The expression of Vps4^{DN} with P35 results in strong punctuate accumulations of GFP-Atg8a.

(F and G) ESCRT mutant cells autonomously accumulate distinct large Hrs-positive endosomes and GFP-Atg8a structures, whereas such structures are not seen in mRFP-positive control cells (blue).

(H) GFP-Atg8a and HRP-Lamp1 accumulate in distinct structures in *vps25* mutant follicle cells.

(I and J) GFP-Atg8a structures largely colocalize with Texas Red dextran (TRD) in control discs (65.0% ± 12.8, n = 655 structures, six discs, six animals), whereas in *vps25* mutant discs, GFP-Atg8a structures are mainly devoid of TRD (98.5% ± 2.3, n = 589 structures, eight discs, five animals). Values are given as ± the standard deviation (SD).

(K) TRD is able to reach the HRP-Lamp1 compartment in *vps25* mutant discs.

(L) Quantification of (I) and (J).

Scale bars represent 2 µm. The genotypes are as follows: *y,w, hs-flp/+;FRT42D, vps28^{D2}/CG-Gal4, FRT42D, UAS-mRFP; UAS-GFP-Atg8a/+* (A), *y,w, hs-flp/+;FRT42D,vps25^{A3}/CG-Gal4, FRT42D, UAS-mRFP; UAS-GFP-Atg8a/+* (B, C, F, and G), *y,w;CG-Gal4,FRT42D,UAS-mRFP/+;UAS-GFP-Atg8a/UAS-P35* (D), *y,w;CG-Gal4, FRT42D, UAS-mRFP/UAS-HA-Vps4^{DN};UAS-GFP-Atg8a/UAS-P35* (E), *y,w, hs-flp/+;FRT42D,vps25^{A3}/CG-Gal4, FRT42D, UAS-mRFP; UAS-GFP-Atg8a/UAS-HRP-Lamp1* (H), *nub-Gal4,UAS-GFPAtg8a* (I), *y,w,* hs-flp/+;FRT42D,vps25^{A3}/FRT42D,Gmr-hid, cl; ey-Gal4,UAS-flp/UAS-GFP-Atg8a (J), and *y,w,* hs-flp/+;FRT42D,vps25^{A3}/FRT42D,Gmr-hid, cl; ey-Gal4,UAS-flp/UAS-HRP-Lamp1 (K). "*" indicates $p < 0.05$, and "**" indicates $p < 0.05$.

and also show that the physiological control of starvation-induced autophagy is still intact in animals containing ESCRT mutant cells.

The AAA ATPase Vps4 (Vps: vacuolar protein sorting) interacts with ESCRT-III components and is necessary for ESCRT-III function, apparently through disassembling multimeric ESCRT-III complexes on the endosomal membrane [21]. An ATPase-deficient version of Vps4 acts like a dominant-negative mutant in endosomal sorting and transport [21]. In agreement with earlier findings in mammalian cells, the expression of a hemagglutinin (HA)-tagged *Drosophila* Vps4^{DN} produced a strong accumulation of GFP-Atg8a in all fat body cells of nonstarved larvae (Figures 2D and 2E) [22]. This indicates that not only ESCRTs but also their disassembling ATPase is required for autophagy.

To investigate the nature of the GFP-Atg8a-containing profiles, we studied wild-type and ESCRT mutant tissues by using established markers of endosomes and lysosomes. In ESCRT mutant cells of *Drosophila*, monoubiquitinated transmembrane receptors destined for degradation in the lysosome accumulate in an endosomal compartment positive for Hrs, a peripheral membrane marker for the sorting endosome [18, 23–25]. In marked contrast to transmembrane receptors, GFP-Atg8a-positive structures in ESCRT mutant or Vps4^{DN}-expressing cells did not colocalize with Hrs (Figures 2F and 2G and Figures S1A–S1D in the Supplemental Data available online), whereas such colocalization was evident in wild-type L3 fat body cells (Figure S1E). These results indicate that the compartments that accumulate transmembrane receptors and GFP-Atg8a in ESCRT mutant cells are distinct.

HRP-Lamp1 (HRP: horseradish peroxidase), a marker for late endosomes and lysosomes, colocalizes with GFP-Atg8 in autolysosomes of wild-type larvae (Figure S1F). In contrast, in *vps25* mutant follicle cells, GFP-Atg8a accumulated in structures distinct from those containing HRP-Lamp1, suggesting a lack of fusion between autophagosomes and endolysosomes in the absence of functional ESCRTs (Figure 2H). Because ESCRT mutations affect the trafficking of a number of transmembrane molecules, it remained possible that HRP-Lamp1 was trapped in a biosynthetic compartment and therefore failed to colocalize with GFP-Atg8a. To bypass this problem, we used Texas Red Dextran (TRD) as a fluid-phase endocytic tracer in eye imaginal discs and asked whether GFP-Atg8a colocalized with TRD-containing endosomal and lysosomal compartments. Control discs showed a low basal amount of autophagy with GFP-Atg8a partially colocalizing with TRD-containing late endosomes and lysosomes, indicating the presence of both autophagosomes and amphisomes or autolysosomes (Figures 2I and 2L). A similar colocalization was observed in L3 fat body cells, which contain more autophagic activity (Figure S1G). Similar to follicle and fat body cells, a strong GFP-Atg8a accumulation was observed in mutant discs consisting almost exclusively of *vps25* mutant cells (Figure 2J). In contrast to the situation in control discs, GFP-Atg8a did not colocalize with TRD in the *vps25* mutant cells. This suggests a lack of fusion of endolysosomal and autophagosomal compartments in the mutant cells (Figures 2J and 2L). The lack of colocalization in *vps25* mutant discs was not due to impaired uptake or trafficking because TRD reached structures labeled with HRP-Lamp1 (Figure 2K). This finding also confirms that HRP-Lamp1 labels endocytic compartments in *vps25* mutant cells. Taken together, our results suggest that ESCRT and Vps4 functions are required for the fusion of autophagic structures with the endolysosomal pathway.

In order to characterize the structures accumulating in larvae with impaired ESCRT, Vps4, or Fab1 function at the ultrastructural level, we investigated mutant larvae by electron microscopy, which stringently identifies the presence of autophagosomes. As previously reported, few autophagic structures were apparent in the fat body cells or the epithelial cells of the gut in L2 larvae (Figures 3A, 3E, and 3J and Figure S2C) [14]. Larvae mutant for *vps28* or *vps25*, on the other hand, accumulated massive amounts of autophagosomes in both the gut and fat body (Figures 3B, 3C, 3F, 3G, and 3J). In contrast, no amphisomes or autolysosomes were evident, suggesting that the fusion of autophagsomes with late endosomes and/or lysosomes is defective in the absence of *vps28* or *vps25*. In larvae expressing Vps4^{DN} specifically in the fat body and not in the gut epithelium, a strong accumulation of autophagic structures was apparent in fat body cells only (Figures 3D and 3H and Figures S1D and S1E). The Vps4^{DN}-induced autophagic structures were, however, less homogeneous in appearance than those in ESCRT mutant larvae. Although the vast majority of the Vps4^{DN}-induced autophagic structures were clearly autophagosomes, others had morphology consistent with material at various stages of degradation, indicating that some fusion of autophagosomes with endosomes or lysosomes carrying degradative enzymes had occurred. The latter finding suggests a lower penetrance of the Vps4^{DN} phenotype than of ESCRT null mutations and is in agreement with earlier work in which the expression of a mammalian dominant-negative Vps4 homolog, SKD1^{DN}, or the small interfering RNA (siRNA)-mediated depletion of Tsg101 in HeLa cells led to the accumulation of autophagosomes and, to a lesser extent, of autolysosomes [22, 26].

Distinct from cells whose ESCRT or Vps4 function was compromised, cells lacking *fab1* exhibited the accumulation of amphisomes. In eye imaginal discs, these were identified by electron microscopy as vacuolar structures containing endocytosed BSA-gold and undegraded cytoplasmic material (Figure 3I). Morphologically similar structures were observed in *fab1* mutant gut cells (Figures S2A and S2B) but not in ESCRT mutant cells (Figures 3B, 3C, 3F, and 3G). This result indicates that Fab1 is required for the progression of amphisomes to autolysosomes, paralleling its role in the endosomal system, where Fab1 regulates the maturation of late endosomes into lysosomes [20, 27]. We speculate that this lack of progression to autolysosomes might be caused by the failure of acidification of the endosomal compartment [20]. Taken together, our data thus suggest that ESCRT, Vps4, and Fab1 act at distinct consecutive steps during basal autophagy. ESCRT and Vps4 functions are necessary for the autophagosome-endolysosome fusion step, whereas Fab1 function is necessary for the maturation of autolysosomes (Figure 4K).

Autophagy under nonstarvation conditions is thought to be important for the removal of misfolded proteins

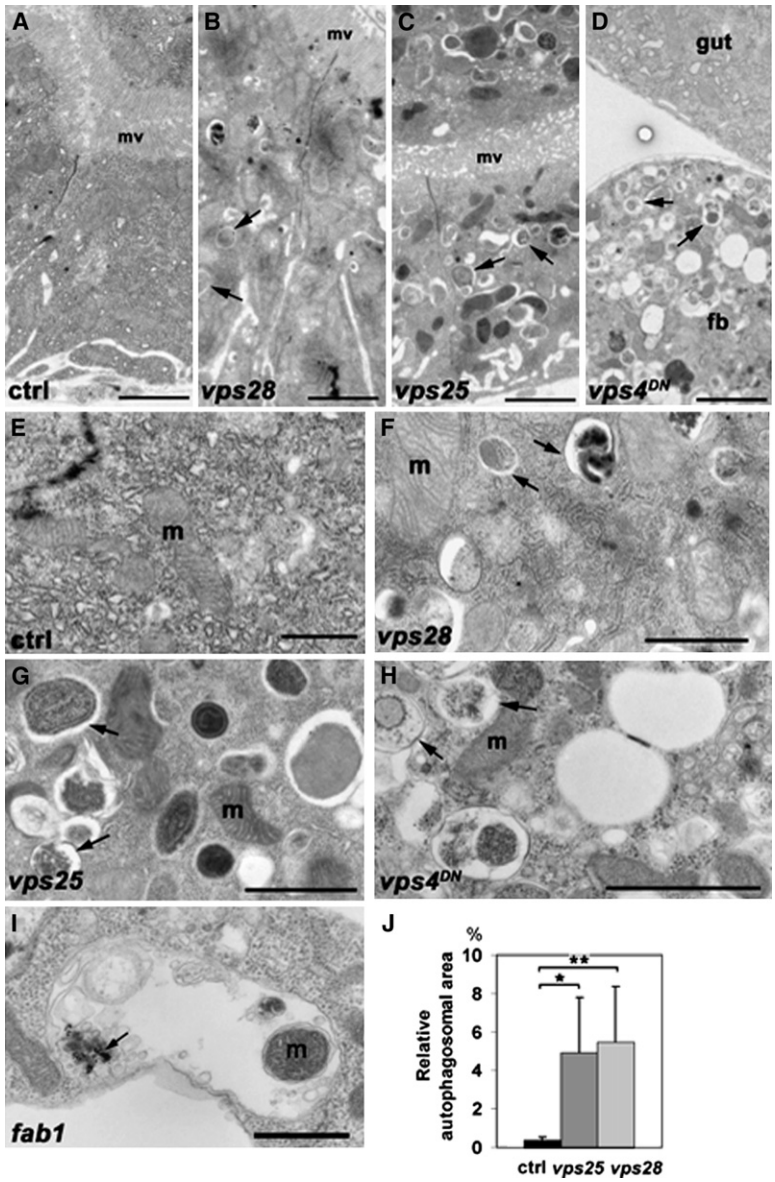

Figure 3. Ultrastructural Analysis of Autophagic Structures in *Drosophila* Larvae with Disrupted ESCRT, Vps4, and Fab1 Function

(A) Gut cells of L1 control larvae have few autophagosomes.

(B, C, F, G, and J) Gut cells of *vps25* and *vps28* L1 larvae show strong accumulation of autophagosomes containing cytoplasmic material (arrows) that can also be observed in the fat body and mosaic eye disks (not shown).

(D and H) Gut cells from L1 larvae expressing $Vps4^{DN}$ in the fat body at 29°C are devoid of autophagy, whereas a strong accumulation of autophagosomes (arrow) are observed in fat body cells.

(E) Enlargement of (A).

(I) Eye disc cells of L3 *fab1* mutant larvae contain large amphisomes characterized by endocytosed BSA-gold (dark punctae, arrow) and autophagic material, including organelles ("m," mitochondrion).

(J) Quantification of (A). The percentage area occupied by autophagic vesicles relative to total cytosol is shown. Values are given as mean of ± the SD. The total cytosolic area quantified was as follows: for w^{1118}, 2629482 μm^2 (six animals), for $vps25^{A3}$, 2419329 μm^2 (six animals), and for $vps28^{D2}$, 2665362 μm^2 (six animals). "*" indicates $p < 0.05$, and "**" indicates $p < 0.05$.

Scale bars represent 2 μm (A–D), 1 μm (E–H), and 500 nm (I). The genotypes are as follows: w^{1118} (A and E), *w;FRT42D,* $vps28^{D2}$ (B and F), *w,FRT42D,*$vps25^{A3}$ (C and G), *y, w, hs-flp/+; CG-Gal4,FRT42D,UAS-mRFP/+;UAS-*$Vps4^{DN}$*/ UAS-GFP-Atg8a* (D and H), and *FRT42D,* $fab1^{21}$*/FRT42D,*$fab1^{31}$ (I).

from the cytoplasm, and impaired autophagy has therefore been postulated to contribute to neurodegenerative diseases in humans. In support of this model, in mice made specifically defective in autophagy in the central nervous system (CNS), brain cells accumulate polyubiquitinated protein aggregates and die [2, 28, 29]. In addition, reducing autophagy aggravates neurotoxicity in models of Huntington's disease in *Drosophila* and *Caenorhabditis elegans*, whereas boosting autophagy can suppress cytotoxicity in these models of polyglutamine-induced protein-aggregate diseases [30–32].

Because our data show that ESCRT proteins are required for autophagy, we asked whether ESCRT proteins have a role in protein-aggregate-induced neurodegeneration by using a *Drosophila* model for Huntington's disease [33–35]. The expression of a 120Q polyglutamine expansion protein specifically in the photoreceptors of the developing eye resulted in a strong reduction in the number of intact photoreceptor neurons (Figures 4A, 4B, and 4G). This provides a sensitized system in which the potential role of ESCRT proteins in the removal of toxic proteins from the cytoplasm can be addressed. Interestingly, removing one copy of either *vps28*, *vps25*, or *vps32* resulted in an increased loss of photoreceptor neurons (Figures 4C–4E and 4H–4J) despite having no toxic effect by itself (Figure S3). We conclude that ESCRT function might be needed for the autophagic clearance of toxic proteins in the cytoplasm in order to protect against neuronal cell death. This is consistent with a paper published when the present manuscript was under review, reporting that impaired ESCRT-III functions cause the death of cultured neurons and the accumulation of autophagosomes [36].

The findings presented here show the cell-autonomous accumulation of autophagosomes in ESCRT mutant cells or in cells expressing $Vps4^{DN}$. This accumulation is most likely explained by a lack of fusion between autophagosomes and endolysosomal compartments during basal autophagy. Alternatively, it could be an indirect effect of upregulation of proautophagic signaling

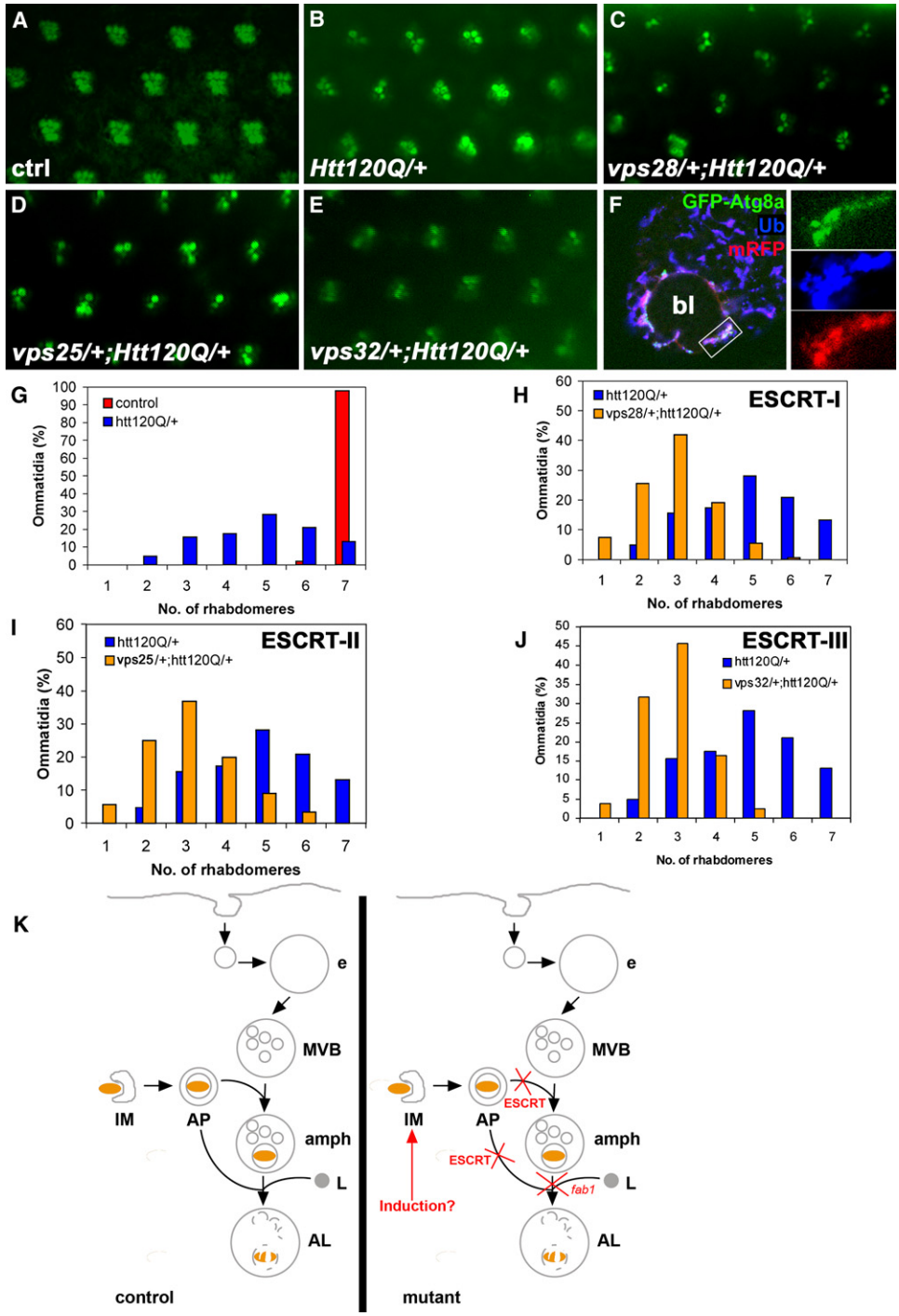

Figure 4. Reduced ESCRT Dosage Aggravates Neurodegeneration of Photoreceptors

(A and B) The majority of ommatidia of control flies contain seven visible photoreceptors 2 days after eclosion, whereas the expression of Htt-Q120 markedly reduced the number of intact photoreceptors.

(C–E) Reducing the gene dosage of *vps28*, *vps25*, or *vps32* led to a further loss of photoreceptors.

(F) $VPS4^{DN}$-expressing neurons (labeled by mRFP) in the larval brain contain ubiquitinated aggregates, a subset of which also colocalize with GFP-Atg8a. The boxed region is showed enlarged in separate channels to the right.

(G) Quantification of (A) and (B).

(H–J) Quantification of (C)–(E).

(K) Model of the function of endocytic regulators during basal autophagy. The normal (control) situation is shown to the left, and the step disrupted in cells deficient of ESCRT/Vps4 or Fab1 function is indicated to the right (red crosses). An induction of autophagy may occur in ESCRT/$Vps4^{DN}$ mutant cells. A double-membraned isolation membrane ("IM") (also called phagophore) can engulf organelles (indicated in brown), cytoplasm, and protein aggregates, forming an autophagosome ("AP"). ESCRT function is needed for the fusion of autophagosomes with the endolysosomal pathway ("e," endosome; "MVB," multivesicular body), whereas *fab1* appears to be necessary for the fusion of amphisomes ("amph") to lysosomes ("l") or a maturation step from amphisomes to the degradative autolysosomes ("AL"). The following abbreviations are also used: brain lobe ("bl") and multivesicular body ("MVB").

or a failure in lysosome biogenesis (Figure 4K). We favor the first possibility because in ESCRT mutant cells, we could observe Hrs-positive sorting endosomes and Lamp1-positive late endosomes or lysosomes but not their fusion products with autophagosomes. This suggests a specific defect in fusion, and this defect could possibly be explained through interference with SNARE function or the failed recruitment of the HOPS-C complex required for this fusion step in yeast and *Drosophila* [37, 38]. The latter hypothesis is supported by the recent finding that ESCRT-I interacts with the HOPS-C subunit Vps18 [39].

Several recent findings suggest a direct involvement of defective ESCRT function in human neurodegenerative disease. A rare inheritable form of the neurodegenerative disease, frontotemporal dementia (FTD), was recently mapped to a dominant mutation in the ESCRT-III member, CHMP2B/Vps2B [4]. Similarly, CHMP2B mutations were observed in patients suffering from amyotrophic lateral sclerosis (ALS) [40]. Motor neurons from affected ALS patients showed protein inclusions labeled with ubiquitin and p62, a protein recently found to be necessary to recruit LC3 (a human Atg8 homolog), suggesting that polyubiquitinated protein aggregates might be tagged for autophagy by p62 in ALS patients or reside in autophagosomes failing to fuse with the endolysosomal pathway. In line with such a model, we observed the accumulation of aggregated ubiquitin-positive structures colocalizing with GFP-Atg8a in $Vps4^{DN}$-expressing neurons in the larval brain (Figure 4F). A further link between ESCRT proteins and neurodegeneration in mammals has been suggested because mice deficient in Mahogunin, an E3 ubiquitin ligase that is necessary for ubiquitination and function of the ESCRT-I subunit, Tsg101, also develop neurodegenerative disease [41, 42]. Strikingly, we found that reduced ESCRT function led to aggravated neurotoxicity in a *Drosophila* Huntington's disease model, thereby providing direct evidence for a neuroprotective role of the ESCRTs. In conclusion, the results presented herein raise the possibility that components of the endosomal sorting machinery could protect against neurodegenerative disease through their function in autophagy.

Experimental Procedures

Fly Strains and Clonal Analysis

The $vps28^{D2}$ and $vps32^{G5}$ alleles were generated by ethylmethane sulfonate (EMS) mutagenesis with a *FRT42D* chromosome. They both behave as null alleles (T.V. and D.B., unpublished data). The $vps25^{A3}$, *FRT42D* chromosome is also a null and is described in [18], $fab1^{21}$ and $fab1^{31}$ are both null alleles [20], *yw,hsflp;CG-Gal4,FRT42D, UAS-mRFP* was a kind gift from T.P. Neufeld, w;UAS-HRP-Lamp1 was provided by Hugo Bellen [25], *Sp/CyO;Gmr-HttQ120/TM6,Tb* was obtained from Bloomington [43], and w; UAS-GFP-Atg8a and w; UAS-$Vps4^{DN}$ are described in this study. All crosses were performed at 25°C except for the overexpression of P35 and/or $Vps4^{DN}$, which was performed at 29°C so that increased expression levels could be allowed. P35 was coexpressed with $Vps4^{DN}$ so that cell death could be counteracted. All other fly lines are described in Bloomington. Overgrown eye discs entirely consisting of $vps25^{A3}$ mutant cells were produced with the *FRT, Gmr-hid* technique in which nonmutant cells are emliminated [18, 44]. For the induction of clones in the fat body embryos, young embryos (0–6 hr after egg deposition) were heat shocked for 1 hr at a 37°C water bath, and let develop into L1 larvae at 25°C. Clones in the follicle cells were induced by the heat shocking of adult female flies for 1 hr at 37°C at day 1, 2, and 3 after hatching. Ovaries were dissected and fixed in 4% formaldehyde in phosphate-buffered saline (PBS) at day 4.

Construction of *HA-Vps4*^{DN} and *GFP-Atg8a* Transgenes

The Vps4 cDNA was amplified by polymerase chain reaction (PCR) from an expressed sequence tag (EST) clone containing CG6842-RA with the following primers: 5′-CCGGAATTCATCACCATGGCAGC CGGTACCAC-3′ (forward) and 5′-CCGCTCGAGCTAAGCGTAATC TGGAACATCGTATGGGTAGCCCTCCTGCCCAAAGTC-3′ (reverse). Nucelotides encoding the HA epitope were appended to the reverse primer so that Vps4-HA was produced. The Vps4-HA fragment was cloned into the EcoRI and XhoI sites of pMT/V5-HisA (Invitrogen). So that Vps4DN-HA would be made, the E232Q mutation was introduced in Vps4-HA with the QuickChange kit from Stratagene, along with the primer 5′-CCCTCCATTATCTTCATTGACCAGATCGATTCG ATGTGCTCGG-3′ and its reverse complement. Both constructs were verified by sequencing and transferred into pUAST at the unique EcoRI and Xho1 sites. *Drosophila* Atg8a (CG32672) was PCR amplified from a complementary DNA (cDNA) clone kindly provided by G. Juhasz. EcoRI and SalI restriction sites were introduced on the 5′ end and 3′ end respectively with the following primers: 5′-GGCAG GAATTCTATGAAGTTCCAATACAAGGAGGAGC-3′ (forward) and 5′-CGAGCCGTCGACTTAGTTAATTTTGGCCATGCCGTAAAC-3′ (reverse). The PCR product was subcloned as an in-frame fusion with eGFP to the vector pEGFP-c1 (Clonetech). The eGFP-DrAtg8a fragment was then PCR amplified with the introduction of the restriction sites Not1 and Xba1 on the 5′ end and 3′ end respectively. The following primers were used: 5′-GCGATCATCGGCGGCCGCATGGTGAGC AAGGGCGAGGAGC-3′ (forward) and 5′-GCCACGGTCTAGATTAGT TAATTTTGGCCATGCCGTAAAC-3′ (reverse). The resulting construct was verified by sequencing and transferred into pUASp with the unique Not1 and Xba1 sites. The final constructs, pUASp-eGFP-DrAtg8a and pUAST-Vps4DN-HA, were introduced in w^{1118} or *yw* flies, respectively, with a standard *P* element transformation protocol.

Texas Red Dextran–BSA-Gold Uptake and Immunohistochemistry

TRD (lysine fixable, MW3000, Molecular Probes) was incubated for 20 min in M3 medium at room temperature with freshly dissected control or overgrown $vps25^{A3}$ mutant eye discs from wandering L3 larvae. The tissues were then transferred to fresh M3 medium for 90 min chase. This protocol allows for the labeling of late endolysosomal compartments [45]. BSA-gold was incubated for 90 min in M3 medium at room temperature with freshly dissected *fab1* mutant eye discs from wandering L3 larvae. Immunochemistry was performed with standard techniques. Guinea pig anti-Hrs (dilution 1:1000) [25] and rabbit anti-HRP (dilution 1:1000) (Sigma) were used.

Pseudopupil Analysis

Pseudopupil analysis allows for the visualization of the rhabdomeres in the ommatidia of the compound eye and was performed essentially as described earlier [46], with the following modifications: Decapitated heads were glued to drops of 1% agarose on a microscope slide with transparent nail varnish. Eyes were analyzed with a Zeiss Axiovert 200M microscope equipped with a 16× objective and photographed with an Axiocam HRm digital camera.

Ultrastructural Analysis

Larvae of the appropriate genotype and stage of development were fixed and processed as described earlier for electron microscopy [14]. Autophagosomes were characterized by the containment of undegraded cytoplasmic material (mitochondria or endoplasmatic reticulum) and a double membrane. Because of a fixation artifact, the latter is often visible as a characteristic halo around the autophagsosome. Autolysosomes were identified as structures with a single

The genotypes and number of ommatidia analyzed are as follows: w^{1118}, n = 97 (A and F), *+/Sp;/+Gmr-HttQ120* (n = 167) (B and F), *Sp/FRT42D,* $vps28^{D2}$*;+/Gmr-HttQ120* (n = 310) (C and G), *Sp/FRT42D,*$vps25^{A3}$*;+/Gmr-HttQ120* (n = 176); (D and H), *Sp/FRT42D,*$vps32^{G5}$*;+/Gmr-HttQ120* (n = 76) (E and I), and *y,w, hs-flp/+; CG-Gal4, FRT42D, UAS-mRFP/UAS-HA-*$Vps4^{DN}$*; UAS-GFP-Atg8a/UAS-P35* (F).

limiting membrane containing partially degraded cytoplasmic components. Vesicular structures containing undegraded cytosolic cargo together with BSA-gold were designated as amphisomes.

Supplemental Data

Three figures are available at http://www.current-biology.com/cgi/content/full/17/20/1817/DC1/.

Acknowledgments

We are very grateful to Thomas P. Neufeld for development of the FLP-FRT technology used in this study and for generously sharing fly lines and experience used for clonal analysis of autophagy in the fat body ahead of publication. Thanks to P.O. Seglen for discussions during the course of the project. We also thank Hugo, J. Bellen, G. Juhasz and Helmut Krämer for reagents and fly lines and J. Lawrence Marsh for advice on the pseudopupil assay. This work was supported by The Norwegian Research Council and Functional Genomics, Norway (T.E.R), the Hartmann Family Foundation, the Norwegian Cancer Society, the Novo Nordisk Foundation, and the American Heart Association (T.V.), the National Institutes of Health and American Cancer Society (D.B.), and the UK's Medical Research Council (F.W. and J.-P.V).

Received: May 16, 2007
Revised: September 16, 2007
Accepted: September 17, 2007
Published online: October 11, 2007

References

1. Levine, B., and Klionsky, D.J. (2004). Development by self-digestion: Molecular mechanisms and biological functions of autophagy. Dev. Cell *6*, 463–477.
2. Komatsu, M., Ueno, T., Waguri, S., Uchiyama, Y., Kominami, E., and Tanaka, K. (2007). Constitutive autophagy: Vital role in clearance of unfavorable proteins in neurons. Cell Death Differ. *14*, 887–894.
3. Berg, T.O., Fengsrud, M., Stromhaug, P.E., Berg, T., and Seglen, P.O. (1998). Isolation and characterization of rat liver amphisomes. Evidence for fusion of autophagosomes with both early and late endosomes. J. Biol. Chem. *273*, 21883–21892.
4. Skibinski, G., Parkinson, N.J., Brown, J.M., Chakrabarti, L., Lloyd, S.L., Hummerich, H., Nielsen, J.E., Hodges, J.R., Spillantini, M.G., Thusgaard, T., et al. (2005). Mutations in the endosomal ESCRTIII-complex subunit CHMP2B in frontotemporal dementia. Nat. Genet. *37*, 806–808.
5. Levine, B. (2007). Cell biology: Autophagy and cancer. Nature *446*, 745–747.
6. Noda, T., and Ohsumi, Y. (2004). Macroautophagy in yeast. In Autophagy, D.J. Klionsky, ed. (Georgetown, Texas: Landes Bioscience), pp. 70–83.
7. Klionsky, D.J., Cregg, J.M., Dunn, W.A., Jr., Emr, S.D., Sakai, Y., Sandoval, I.V., Sibirny, A., Subramani, S., Thumm, M., Veenhuis, M., et al. (2003). A unified nomenclature for yeast autophagy-related genes. Dev. Cell *5*, 539–545.
8. Gutierrez, M.G., Munafo, D.B., Beron, W., and Colombo, M.I. (2004). Rab7 is required for the normal progression of the autophagic pathway in mammalian cells. J. Cell Sci. *117*, 2687–2697.
9. Jager, S., Bucci, C., Tanida, I., Ueno, T., Kominami, E., Saftig, P., and Eskelinen, E.L. (2004). Role for Rab7 in maturation of late autophagic vacuoles. J. Cell Sci. *117*, 4837–4848.
10. Gordon, P.B., and Seglen, P.O. (1988). Prelysosomal convergence of autophagic and endocytic pathways. Biochem. Biophys. Res. Commun. *151*, 40–47.
11. Fengsrud, M., Roos, N., Berg, T., Liou, W., Slot, J.W., and Seglen, P.O. (1995). Ultrastructural and immunocytochemical characterization of autophagic vacuoles in isolated hepatocytes: Effects of vinblastine and asparagine on vacuole distributions. Exp. Cell Res. *221*, 504–519.
12. Li, S., Tiab, L., Jiao, X., Munier, F.L., Zografos, L., Frueh, B.E., Sergeev, Y., Smith, J., Rubin, B., Meallet, M.A., et al. (2005). Mutations in PIP5K3 are associated with Francois-Neetens mouchetee fleck corneal dystrophy. Am. J. Hum. Genet. *77*, 54–63.
13. Scott, R.C., Schuldiner, O., and Neufeld, T.P. (2004). Role and regulation of starvation-induced autophagy in the Drosophila fat body. Dev. Cell *7*, 167–178.
14. Rusten, T.E., Lindmo, K., Juhâasz, G., Sass, M., Seglen, P.O., Brech, A., and Stenmark, H. (2004). Programmed autophagy in the Drosophila fat body is induced by ecdysone through regulation of the PI3K pathway. Dev. Cell *7*, 179–192.
15. Golic, K.G., and Lindquist, S. (1989). The FLP recombinase of yeast catalyzes site-specific recombination in the Drosophila genome. Cell *59*, 499–509.
16. Brand, A.H., and Perrimon, N. (1993). Targeted gene expression as a means of altering cell fates and generating dominant phenotypes. Development *118*, 401–415.
17. Kabeya, Y., Mizushima, N., Ueno, T., Yamamoto, A., Kirisako, T., Noda, T., Kominami, E., Ohsumi, Y., and Yoshimori, T. (2000). LC3, a mammalian homologue of yeast Apg8p, is localized in autophagosome membranes after processing. EMBO J. *19*, 5720–5728.
18. Vaccari, T., and Bilder, D. (2005). The Drosophila tumor suppressor vps25 prevents nonautonomous overproliferation by regulating notch trafficking. Dev. Cell *9*, 687–698.
19. Sevrioukov, E.A., Moghrabi, N., Kuhn, M., and Kramer, H. (2005). A mutation in dVps28 reveals a link between a subunit of the endosomal sorting complex required for transport-I complex and the actin cytoskeleton in Drosophila. Mol. Biol. Cell *16*, 2301–2312.
20. Rusten, T.E., Rodahl, L.M., Pattni, K., Englund, C., Samakovlis, C., Dove, S., Brech, A., and Stenmark, H. (2006). Fab1 phosphatidylinositol 3-phosphate 5-kinase controls trafficking but not silencing of endocytosed receptors. Mol. Biol. Cell *17*, 3989–4001.
21. Babst, M., Wendland, B., Estepa, E.J., and Emr, S.D. (1998). The Vps4p AAA ATPase regulates membrane association of a Vps protein complex required for normal endosome function. EMBO J. *17*, 2982–2993.
22. Nara, A., Mizushima, N., Yamamoto, A., Kabeya, Y., Ohsumi, Y., and Yoshimori, T. (2002). SKD1 AAA ATPase-dependent endosomal transport is involved in autolysosome formation. Cell Struct. Funct. *27*, 29–37.
23. Thompson, B.J., Mathieu, J., Sung, H.H., Loeser, E., Rørth, P., and Cohen, S.M. (2005). Tumor suppressor properties of the ESCRT-II complex component Vps25 in drosophila. Dev. Cell *9*, 711–720.
24. Moberg, K.H., Schelble, S., Burdick, S.K., and Hariharan, I.K. (2005). Mutations in erupted, the Drosophila ortholog of mammalian tumor susceptibility gene 101, elicit non-cell-autonomous overgrowth. Dev. Cell *9*, 699–710.
25. Lloyd, T.E., Atkinson, R., Wu, M.N., Zhou, Y., Pennetta, G., and Bellen, H.J. (2002). Hrs regulates endosome membrane invagination and tyrosine kinase receptor signaling in Drosophila. Cell *108*, 261–269.
26. Doyotte, A., Russell, M.R., Hopkins, C.R., and Woodman, P.G. (2005). Depletion of TSG101 forms a mammalian "Class E" compartment: A multicisternal early endosome with multiple sorting defects. J. Cell Sci. *118*, 3003–3017.
27. Nicot, A.S., Fares, H., Payrastre, B., Chisholm, A.D., Labouesse, M., and Laporte, J. (2006). The phosphoinositide kinase PIKfyve/Fab1p regulates terminal lysosome maturation in Caenorhabditis elegans. Mol. Biol. Cell *17*, 3062–3074.
28. Hara, T., Nakamura, K., Matsui, M., Yamamoto, A., Nakahara, Y., Suzuki-Migishima, R., Yokoyama, M., Mishima, K., Saito, I., Okano, H., et al. (2006). Suppression of basal autophagy in neural cells causes neurodegenerative disease in mice. Nature *441*, 885–889.
29. Komatsu, M., Waguri, S., Chiba, T., Murata, S., Iwata, J., Tanida, I., Ueno, T., Koike, M., Uchiyama, Y., Kominami, E., et al. (2006). Loss of autophagy in the central nervous system causes neurodegeneration in mice. Nature *441*, 880–884.
30. Jia, K., Hart, A.C., and Levine, B. (2007). Autophagy genes protect against disease caused by polyglutamine expansion proteins in Caenorhabditis elegans. Autophagy *3*, 21–25.
31. Ravikumar, B., Vacher, C., Berger, Z., Davies, J.E., Luo, S., Oroz, L.G., Scaravilli, F., Easton, D.F., Duden, R., O'Kane, C.J., et al.

(2004). Inhibition of mTOR induces autophagy and reduces toxicity of polyglutamine expansions in fly and mouse models of Huntington disease. Nat. Genet. *36*, 585–595.

32. Berger, Z., Ravikumar, B., Menzies, F.M., Oroz, L.G., Underwood, B.R., Pangalos, M.N., Schmitt, I., Wullner, U., Evert, B.O., O'Kane, C.J., et al. (2006). Rapamycin alleviates toxicity of different aggregate-prone proteins. Hum. Mol. Genet. *15*, 433–442.
33. Kazemi-Esfarjani, P., and Benzer, S. (2000). Genetic suppression of polyglutamine toxicity in Drosophila. Science *287*, 1837–1840.
34. Marsh, J.L., Walker, H., Theisen, H., Zhu, Y.Z., Fielder, T., Purcell, J., and Thompson, L.M. (2000). Expanded polyglutamine peptides alone are intrinsically cytotoxic and cause neurodegeneration in Drosophila. Hum. Mol. Genet. *9*, 13–25.
35. Marsh, J.L., and Thompson, L.M. (2006). Drosophila in the study of neurodegenerative disease. Neuron *52*, 169–178.
36. Lee, J.A., Beigneux, A., Ahmad, S.T., Young, S.G., and Gao, F.B. (2007). ESCRT-III Dysfunction causes autophagosome accumulation and neurodegeneration. Curr. Biol. *17*, 1561–1567.
37. Lindmo, K., Simonsen, A., Brech, A., Finley, K., Rusten, T.E., and Stenmark, H. (2006). A dual function for Deep orange in programmed autophagy in the Drosophila melanogaster fat body. Exp. Cell Res. *312*, 2018–2027.
38. Pulipparacharuvil, S., Akbar, M.A., Ray, S., Sevrioukov, E.A., Haberman, A.S., Rohrer, J., and Krèamer, H. (2005). Drosophila Vps16A is required for trafficking to lysosomes and biogenesis of pigment granules. J. Cell Sci. *118*, 3663–3673.
39. Kim, B.Y., and Akazawa, C. (2007). Endosomal trafficking of EGFR regulated by hVps18 via interaction of MVB sorting machinery. Biochem. Biophys. Res. Commun. Published online August 20, 2007. 10.1016/j.bbrc.2007.08.046.
40. Parkinson, N., Ince, P.G., Smith, M.O., Highley, R., Skibinski, G., Andersen, P.M., Morrison, K.E., Pall, H.S., Hardiman, O., Collinge, J., et al. (2006). ALS phenotypes with mutations in CHMP2B (charged multivesicular body protein 2B). Neurology *67*, 1074–1077.
41. Kim, B.Y., Olzmann, J.A., Barsh, G.S., Chin, L.S., and Li, L. (2007). Spongiform neurodegeneration-associated E3 ligase Mahogunin ubiquitylates TSG101 and eegulates rndosomal trafficking. Mol. Biol. Cell *18*, 1129–1142.
42. He, L., Lu, X.Y., Jolly, A.F., Eldridge, A.G., Watson, S.J., Jackson, P.K., Barsh, G.S., and Gunn, T.M. (2003). Spongiform degeneration in mahoganoid mutant mice. Science *299*, 710–712.
43. Jackson, G.R., Salecker, I., Dong, X., Yao, X., Arnheim, N., Faber, P.W., MacDonald, M.E., and Zipursky, S.L. (1998). Polyglutamine-expanded human huntingtin transgenes induce degeneration of Drosophila photoreceptor neurons. Neuron *21*, 633–642.
44. Stowers, R.S., and Schwarz, T.L. (1999). A genetic method for generating Drosophila eyes composed exclusively of mitotic clones of a single genotype. Genetics *152*, 1631–1639.
45. Entchev, E.V., Schwabedissen, A., and Gonzalez-Gaitan, M. (2000). Gradient formation of the TGF-beta homolog Dpp. Cell *103*, 981–991.
46. Steffan, J.S., Bodai, L., Pallos, J., Poelman, M., McCampbell, A., Apostol, B.L., Kazantsev, A., Schmidt, E., Zhu, Y.Z., Greenwald, M., et al. (2001). Histone deacetylase inhibitors arrest polyglutamine-dependent neurodegeneration in Drosophila. Nature *413*, 739–743.